International Journal of Solids and Structures 50 (2013) 981–995

Contents lists available at SciVerse ScienceDirect

International Journal of Solids and Structures

journal homepage: www.elsevier.com/locate/ijsolstr

Finite element simulation of the pressure dip in sandpiles

Jun Ai [a,b], Jian-Fei Chen [b,*], Jin Y. Ooi [b]

[a] Nottingham Centre for Geomechanics, The University of Nottingham, University Park, Nottingham NG7 2RD, UK
[b] Institute for Infrastructure and Environment, Joint Research Institute for Civil and Environmental Engineering, School of Engineering, The University of Edinburgh, Edinburgh EH9 3JL, Scotland, UK

ARTICLE INFO

Article history:
Received 22 April 2011
Received in revised form 18 October 2012
Available online 19 December 2012

Keywords:
Sandpile
Stockpile
Granular material
Base pressure
Pressure dip
Arching effect
Base shear
Progressive construction
Finite element method

ABSTRACT

Many industrial bulk solids are commonly stored in open stockpiles that are progressively formed by depositing from above. A classic phenomenon concerning such simple piles is the observation of a significant pressure dip in the vertical pressure on the base underneath the apex which is counter-intuitive as this is the location where a maximum pressure might be expected. Numerous experimental, analytical and numerical studies have been conducted to investigate this problem over the last few decades, but a comprehensive understanding of the problem remains elusive. Mechanical anisotropy developed during pile formation process has recently been suggested to be the main cause of the pressure dip. However, more recent finite element method (FEM) studies have predicted a pressure dip beneath the apex using isotropic material models. The review of the literature shows a lack of understanding of the underlying mechanism and the roles of various factors on the prediction of the pressure dip, such as the progressive mesh activation, stress dependency of modulus and plastic failure parameters. The aim of this paper is to investigate the effects of these factors by modelling a set of conical sandpile experiments formed on a rigid base by concentrated deposition. The results show that significant pressure dip can be predicted without considering material anisotropy. However, within the realm of elasto-plastic models investigated, it appears that the prediction of pressure dip requires a model considering the construction process and the associated plastic deformation. Incorporating stress-hardening elasticity enhances significantly the extent of the dip. The results demonstrate that a greater mobilisation of the base shear traction is an important mechanism in enhancing the arching effect that leads to a significant central pressure dip.

1. Introduction

Conical piles of granular solids can be found in many industrial sites. These piles are usually progressively formed by depositing from above. A classic phenomenon concerning such simple piles is the observation that the pressure distribution beneath the pile shows a marked local minimum beneath the apex (Fig. 1) which is often referred to as a "pressure dip". This observation is counter-intuitive as this would be the location expected to have the maximum pressure. Although this "sandpile problem" has mostly been studied as an interesting scientific anomaly (Cates et al. 1998), it does have significant economic importance in terms of bulk solid stockpiles in industry. The solid is often recovered using a retrieving feeder beneath the stockpile, which means that one aspect of stockpile design is to determine the base pressure distribution.

Despite many studies by both the physics and engineering communities over several decades, a comprehensive understanding of the counter-intuitive phenomenon of pressure dip remains elusive. Good reviews of previous analytical, numerical and experimental studies of the problem can be found elsewhere (Savage 1997; Cates et al. 1998; Savage 1998; Atman et al. 2005) and will not be repeated here. Early theoretical studies on the sandpile problem have mostly adopted analytical continuum approaches (e.g., Wittmer et al. 1996), analytical microscopic models (e.g., Liffman et al. 1994; Huntley 1999) or discrete element method (DEM) (e.g., Luding 1997; Matuttis 1998), with very few adopting the finite element method (FEM).

As a deduction of a heated debate on the fundamental laws of force transmissions in granular materials (de Gennes 1999; Goldenberg and Goldhirsch 2005; Luding 2005), it is argued that the mechanical anisotropy (direction dependent properties) should be responsible for the pressure dip phenomenon. Goldenberg and Goldhirsch (2008) concluded that the presence or absence of a dip is determined by the degree of anisotropy in the mechanical properties which depend on the way the pile is constructed. Indeed, numerical modelling adopting anisotropic material models

* Corresponding author. Tel.: +44 131 650 6768; fax: +44 131 650 6781.
E-mail address: j.f.chen@ed.ac.uk (J.F. Chen).

0020-7683/$ - see front matter © 2012 Elsevier Ltd. All rights reserved.
http://dx.doi.org/10.1016/j.ijsolstr.2012.12.006

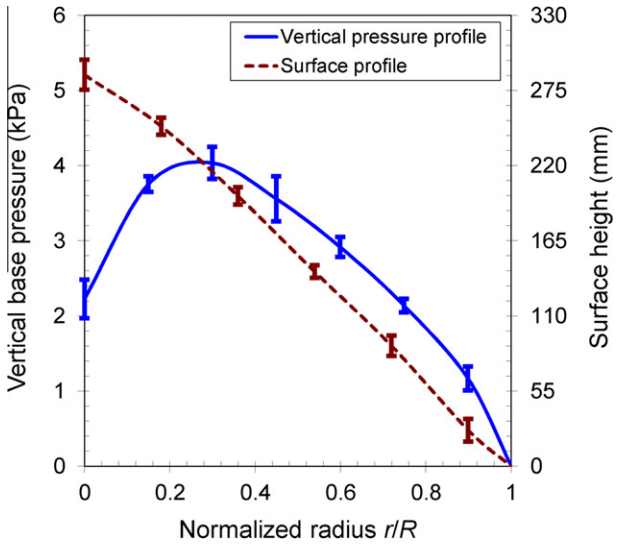

Fig. 1. Vertical base pressure underneath a conical pile of small iron ore pellets (redrawn after Ooi et al. 2008).

have been shown capable of predicting a pressure dip. For example, Savage (1998) suggested that the material properties resulted from avalanching during the pile construction may show different modulus in the plane parallel to the free surface from that in the direction perpendicular to it. His simulation adopting an anisotropic elastic model successfully produced a significant pressure dip. This approach was further supported by experimental evidence by Atman et al. (2005) who adopted parameters deduced from test and simulated a clear dip although it is smaller than that from experiment.

In contrast, several FEM studies have also predicted a pressure dip beneath the apex using elasto-plastic material models without the inclusion of apparent material anisotropy. Anand and Gu (2000) conducted elastic–plastic calculations of a conical pile using the "double-shearing" constitutive model implemented through an explicit code. Following the Mohr–Coulomb yield condition, the angle from the maximum principal stress direction to the slip direction in their formulation was defined as $\xi = \pm\pi/4 \pm \Phi/2$, where Φ is the internal friction angle of the solid. Additional slumping of the pile occurred during the settling process because the initial slope angle was intentionally set larger than the maximum mobilized internal friction angle. The predicted vertical stress distribution showed a clear dip under the apex. The simulated plastic shear strain was small close to the top surface and the core of the pile, but large in between. They concluded that the cause of the dip was the non-homogeneous plastic strain that occurred during the process of the slumping, coupled with the evolution of the internal friction coefficient.

Al Hattamleh et al. (2005) employed a multi-slip formulation of double-shearing type constitutive model in their granular heap calculation. Based on the idea that the initial slip direction is very much dependent on the granular microstructure relating to factors such as depositional history and angularity, the initial slip direction measured from the principal direction was treated as a material parameter rather than fixed. The construction of the granular heap was simulated incrementally in five stages. Calculations with different initial slip directions were carried out, and very pronounced stress dips were predicted in all cases except the one with $\xi = \pm\pi/4 \pm \alpha/2$, where α is the angle of repose of the pile and was set equal to the internal friction angle at constant volume state Φ_{cv}. They predicted localized plastic strain around the apex with the rest of the pile in an elastic state and argued that strain localization is the main cause of the pressure dip.

Examples of successful prediction of pressure dip also include Modaressi et al. (1999) and Tejchman and Wu (2008). The former predicted a significant pressure dip using Hujeux's model (Aubry et al., 1982), and the latter used a micro-hypoplasticity model (Wu et al. 1996) which considers the effect of the direction of deformation rate. Both considered the construction history by modelling the pile in several successive inclined layers.

Whilst the above mentioned FEM studies adopted more complex elasto-plastic models, some other studies have shown that a pressure dip can also be predicted by adopting simpler elastic–plastic models. For example, Modaressi et al. (1999) predicted a small dip using the associated Drucker–Prager model. Jeong and Moore (2010) adopted a Mohr–Coulomb model with Janbu type stress-dependent modulus (Janbu 1963) and predicted a dip with its size comparable to previous experimental observations (Smid and Novosad 1981; Vanel et al. 1999; McBride 2006). Their results were very sensitive to the number of construction layers and the Poisson's ratio adopted in the FEM computations.

Though a pressure dip has been predicted in aforementioned FEM studies, the underlying mechanism of the emergent dip during the FEM pile modelling process is still largely unclear. For example, in some studies the construction history of a pile was implicated by means of elastic anisotropy (Savage 1998; Atman et al. 2005). In other studies, the construction history was explicitly modelled by either including some small slumping during the pile settling process (Anand and Gu 2000), or using progressive mesh activation scheme (Modaressi et al. 1999; Al Hattamleh et al. 2005; Tejchman and Wu 2008; Jeong and Moore 2010). Al Hattamleh et al. (2005) also additionally introduced initial weak planes to further reflect the effect of construction history. These studies using different FE modelling procedures have predicted different plastic strain distributions, and proposed different causes for the pressure dip. There may be some links between all these mechanisms, which are not at all clear. There are also uncertainties in the relative importance of elastic parameters and plastic parameters. Since sophisticated constitutive models often involve a large number of parameters, it is difficult to distinguish their roles in the predicted behaviour.

The aim of this study is to investigate the roles of several key factors that are most probable in affecting the pressure dip phenomenon. These include progressive mesh activation, stress dependency of modulus and the role of plasticity in producing the pressure dip. This study is limited to piles formed on a rigid base by concentrated deposition where the "pressure dip" is more likely present. By adopting isotropic constitutive models, material anisotropy was intentionally excluded to test whether it is indispensible for a pressure dip. Simple general elastic and elasto-plastic models were chosen so that the roles of basic elastic and plastic parameters in producing the numerical solution can be explored more clearly.

2. Finite element modelling

2.1. Reference test pile

The conical pile test conducted by Ooi et al. (2008) with mini iron ore pellets centrally poured on a rigid base was used as reference data in this study. Fig. 1 shows the measured normal base pressure distribution. The pile had a mean radius of $R_p = 0.554$ m and angle of repose of $\alpha = 29°$. The pellets had very rough surface and were relatively uniform in size with a mean diameter of $d_p = 3$ mm. They were approximately spherical and had a relatively uniform bulk density which was relatively insensitive to packing. The loosest and densest bulk densities achieved in control tests were 2260 and 2370 kg/m^3. A bulk density of $\rho = 2260$ kg/m^3

was adopted in the simulations because the pile was small and the particles underwent intensive surface shear flow during the formation process leading to a relatively loose packing.

2.2. Progressive mesh activation scheme

The progressive mesh activation scheme has been adopted previously by the silo research community (e.g., Rotter et al. 1998; Holst et al. 1999; Yu, 2004) and geotechnical researchers (e.g., Clough and Woodward 1967; Kulhawy and Duncan 1972; Rowe and Skinner 2001). The numerical implementation of such a progressively layering process is achieved by discretising the final geometry of the model into many layers in the FE mesh, with each layer activated in the FE computation in a sequence consistent to the construction history. The complete mesh for the final geometry is generated at the beginning, but the gravity and stiffness for all layers are switched off ("deactivated"). The stiffness for the lowest layer is then activated and its gravity gradually applied. Once equilibrium of the layer is reached, the next layer up is activated (in stiffness) in a "strain/stress-free" state, and its gravity gradually applied. Computation is continued until equilibrium is reached for the structure consisting of the current active layer and all layers below it. The layer above the current active layer is then activated. The process continues until all the layers are activated and the whole structure reaches equilibrium.

Considering the modelling procedure of such a scheme and its difference from the "switched-on" loading have not been clearly presented elsewhere, a benchmark test example is presented in the Appendix. The example for an elastic rectangular body under its own gravity shows that the switched-on gravity procedure can produce significant horizontal stresses in the body. Whilst this is real if the body is formed as a whole in one step, it is wrong if the body is formed in a progressive manner in which case the horizontal stress should be zero. The progressive mesh activation scheme can effectively reduce this horizontal stress, and eventually eliminate it if numerous of construction layers are used. Sandpiles are obviously formed progressively, and thus a progressive mesh activation scheme is necessary.

The application of this scheme to the sandpile modelling is based on the observation that during a pile formation process, particles are settled in successive inclined layers (Fig. 2), with the earlier layers being deformed under their own weight before the next layer is laid on. Fig. 2 shows such layered pattern in an example "two dimensional" thin planar pile. The pattern for three dimensional conical piles shall be similar.

2.3. Numerical implementation of pile construction

In this simulation, the sandpile was modelled as a static axisymmetric problem, so the effect of inertia was neglected and the pile was assumed to be axisymmetric during the whole formation process. All calculations were performed using Abaqus/Standard v6.9 (SIMULIA 2007).

The final geometry of the pile was discretised into a number of layers with the innermost cone as the first "layer". Fig. 3 shows an example FE mesh with five layers of elements ($N_{el} = 5$) representing five successive construction layers ($N_{cl} = 5$). Abaqus element type CAX6 was adopted. The bottom boundary of the pile was fixed in both horizontal and vertical direction, representing a rough and rigid base in a physical test. All construction layers are of constant thickness and inclined at the angle of repose (29°). The dynamic effect of particle impacting, flowing and avalanching during the deposition process is neglected.

It is also worth noting, in the mesh pattern of an earlier study (Ai et al. 2009), the central base node only had connectivity to a single triangular element, which was found to give a poor stress evaluation at the node (a central kink in the predicted stress distribution). In the mesh adopted in this study (Fig. 3), the central base node has connectivity with two triangular elements, which was found to be able to effectively eliminate the above central kink phenomenon.

2.4. Constitutive models and parameters

Five well-known constitutive laws for granular solid, including two elastic models and three elastic–plastic models, were explored in this study. They are: (1) linear elastic (LE); (2) porous elastic (PE); (3) linear elastic with Mohr–Coulomb plasticity (LEMC); (4) linear elastic with Drucker–Prager plasticity (LEDP) and (5) porous elastic with Drucker–Prager plasticity (PEDP). These models have been successfully applied to model many granular solids problems in previous studies (e.g., Ooi et al. 1996; Ooi and She 1997; Holst

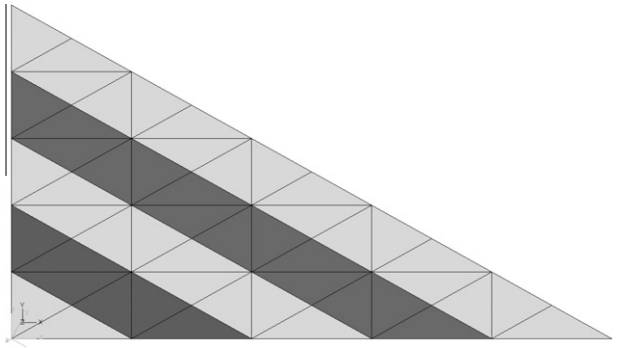

Fig. 3. FE mesh with $N_{el} = N_{cl} = 5$ to simulate progressive sandpile formation.

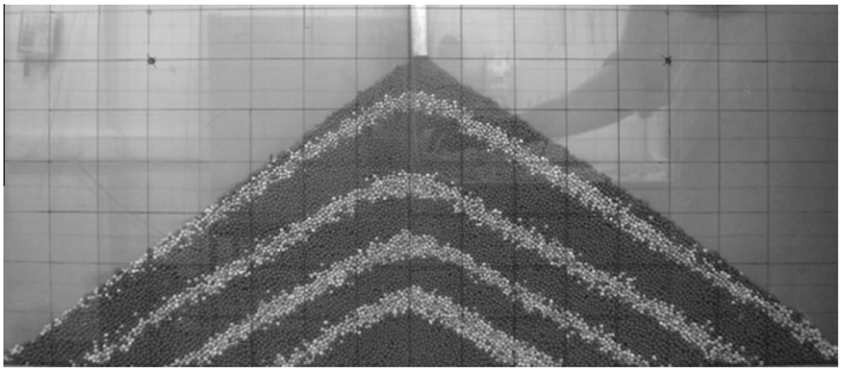

Fig. 2. Layering pattern during the formation of a thin planar test pile. The particles were centrally deposited into a narrow space confined by two transparent Perspex walls. The particles were mini iron ore pellets that were generically black in colour, but some of them were dyed white before deposition. We repeatedly deposit a certain amount of black particles and followed by white particles to produce the layering effect.

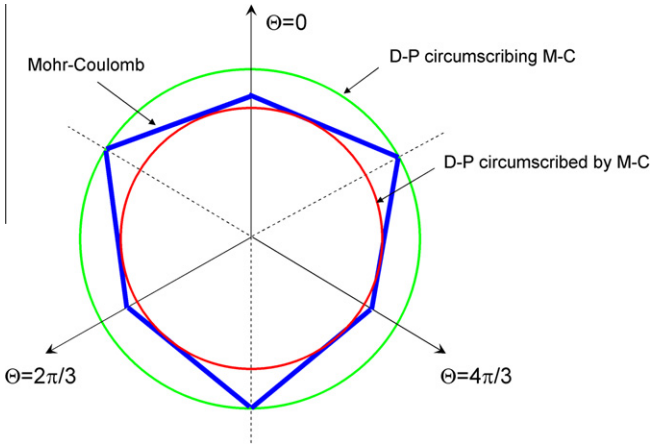

Fig. 4. Mohr–Coulomb (M-C) and Drucker–Prager (D-P) yield surfaces in the deviatoric plane.

et al. 1999; Chen et al. 2001; Goodey et al. 2003; Goodey et al. 2006). The formulation of these models and selection of their parameters are briefly introduced below. Terminology for the model parameters as in Abaqus is adopted.

2.4.1. Linear elastic model and parameters

Earlier studies have shown that the magnitude of the Young's modulus has negligible effect on the prediction of stresses in granular solids in many situations (e.g., Rotter et al. 1998; Savage 1998). The Young's modulus for the linear elastic model was chosen as 2.0 MPa. The Poisson's ratio ν has been shown to be an important parameter (e.g., Ooi and Rotter 1990) but it is not easy to measure. The common values adopted in these studies, however, were not far from 0.3. In this study, $v = 0.3$ was chosen as the reference value while a parametric study is conducted to investigate its effect later in this paper.

2.4.2. Porous elastic model and parameters

The porous elastic model is a nonlinear, isotropic, elastic model in which the equivalent pressure stress (also often referred as the mean stress or the hydrostatic stress) $p = -(\sigma_1 + \sigma_2 + \sigma_3)/3$ varies as an exponential function of the volumetric strain:

$$\frac{\kappa}{1-e_0}\ln\left(\frac{p_0+p_t^{el}}{p+p_t^{el}}\right) = J^{el} - 1 \tag{1}$$

where $J^{el} - 1$ is the nominal volumetric strain; κ is the logarithmic bulk modulus and e_0 is the initial void ratio of the solid; p_0 and p_t^{el} are the initial values of the equivalent pressure stress in the solid and the elastic tensile stress limit of the solid respectively. This model allows either a zero or nonzero elastic tensile stress limit, p_t^{el}. The incremental deviatoric stress tensor $d\boldsymbol{S}$ is related to the incremental deviatoric part of the total elastic strain $d\boldsymbol{e}^{el}$, through

$$dS = 2Gde^{el} \tag{2}$$

where G is the instantaneous shear modulus, given by

$$G = \frac{3(1-2v)(1+e_0)}{2(1+v)\kappa}(p+p_t^{el})J^{el} \tag{3}$$

In this study, the Poisson's ratio v is deemed to be constant in the elastic range, so that the elastic shear stiffness increases as the material is compacted. The relationship between the tangent elastic modulus and the equivalent pressure stress p is therefore given as

$$E = 2G(1+v) = \frac{3(1-2v)(1+e_0)}{\kappa}(p+p_t^{el})\left(1+\frac{k}{1+e_0}\ln\left(\frac{p_0+p_t^{el}}{p+p_t^{el}}\right)\right) \tag{4}$$

Eqs. (1) and (4) mean that $p_0 + p_t^{el}$ must not equal zero for the model to work. Ideally, for cohesionless dry granular solids, the elastic tensile stress limit p_t^{el} should be zero. It is feasible to adopt a zero p_t^{el} in most soil mechanics problems because soil samples

Table 1
Principal parameters used in FE calculations.

Parameter	Symbol	Value	Unit
Density	ρ	2260	kg/m^3
Pile radius	R_p	554	mm
Angle of repose	α	29	°
Elastic modulus	E	2.0	MPa
Poisson's ratio	v	0.3	
Initial void ratio	e_0	1	
Tensile limit	p_t^{el}	10	Pa
Log. bulk modulus	κ	0.002	
Initial stress	p_0	0	Pa
MC friction angle	Φ	29	°
MC dilation angle	ψ	20	°
MC cohesion	c	1	Pa
DP friction angle	Φ_{dp}	45	°
DP dilation angle	ψ_{dp}	20	°
DP cohesion	c_{dp}	1	Pa

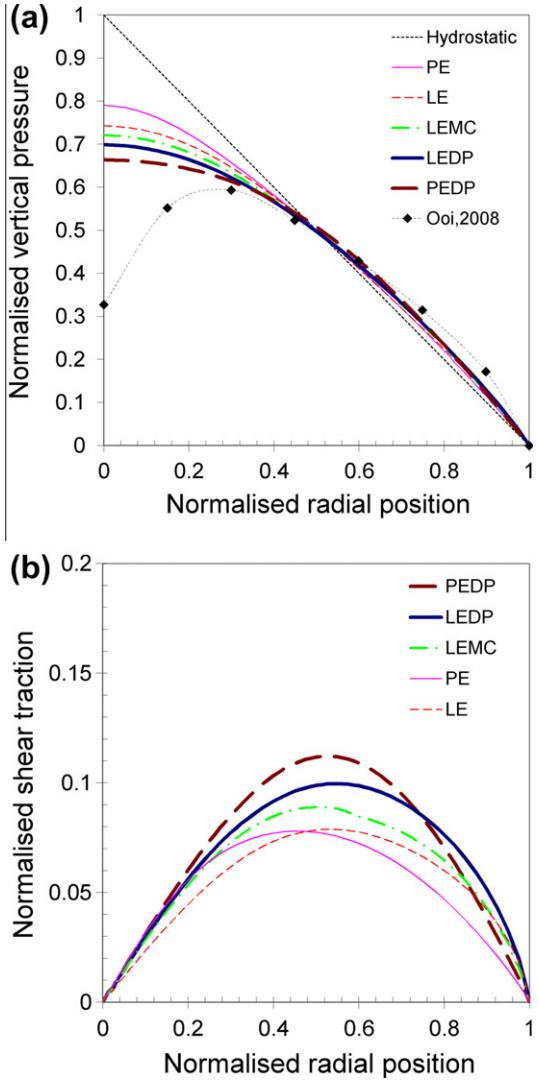

Fig. 5. Base pressure distribution under switched-on gravity ($N_{cl} = 1$). (a) vertical pressure; (b) shear traction.

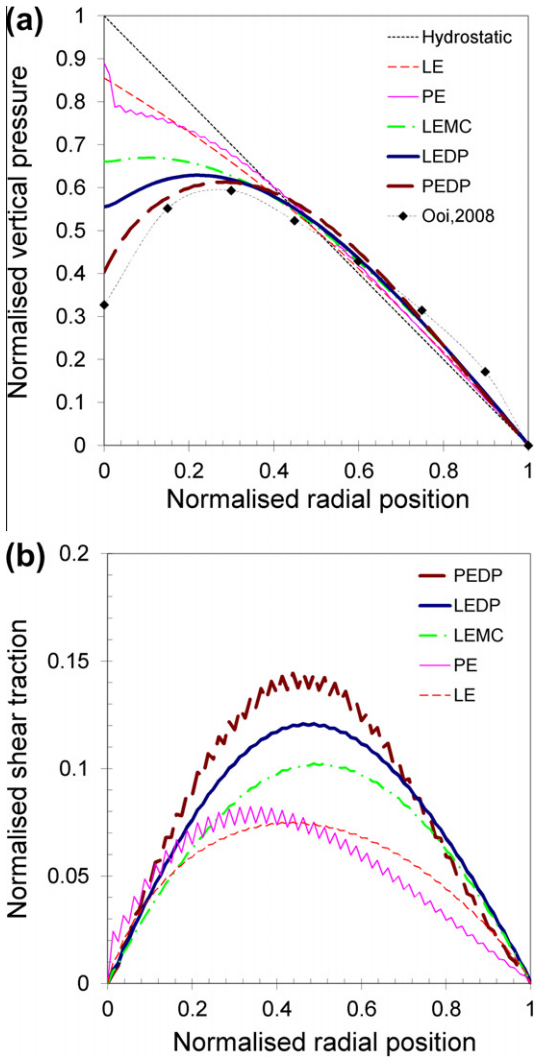

Fig. 6. Base pressure distributions in pile formed by progressive mesh activation (N_{cl} = 40). (a) vertical pressure; (b) shear traction.

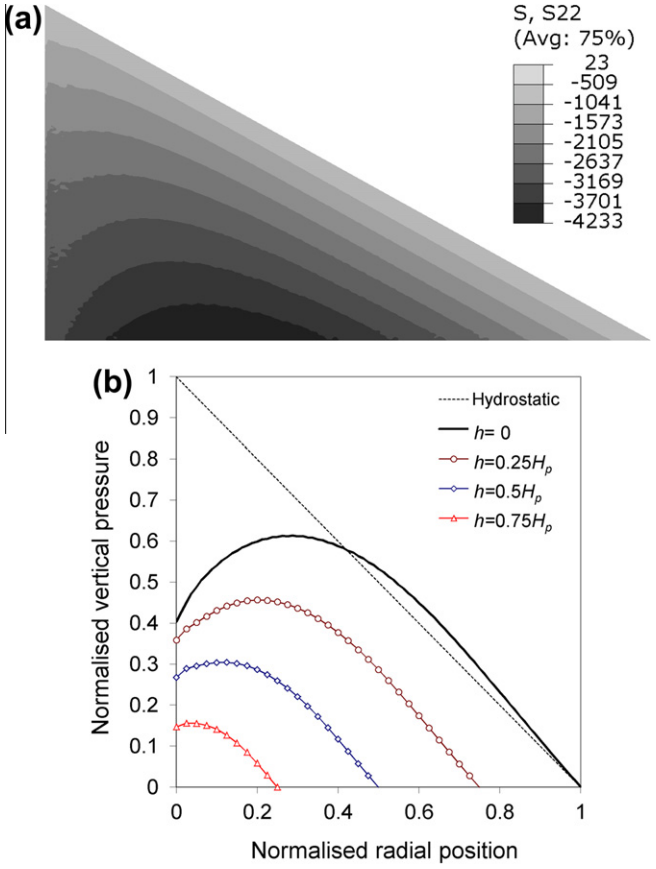

Fig. 8. Vertical stress distribution in pile (unit: Pa). (a) contour of vertical stress distribution; (b) vertical stress distribution at different heights.

are usually in a pre-stressed state so the value of p_0 is not zero. However, it is not applicable to current sandpile formation modelling since the initial stress should be zero. As one of the two values must be nonzero, in the sandpile calculations conducted in this study, p_0 was set as zero and a very small value of p_t^{el} = 10 Pa was chosen. The sensitivity of the results to the value of P_t^{el} is explored later in this paper.

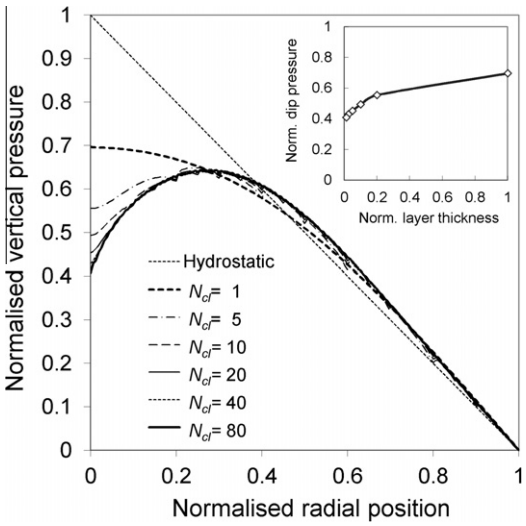

Fig. 7. Effect of number of construction layers on base vertical pressure distribution with PEDP model ($N_{el} = N_{cl}$). Main panel: vertical base pressure profiles. Inset: dip pressure versus the layer thickness normalised against the final pile size.

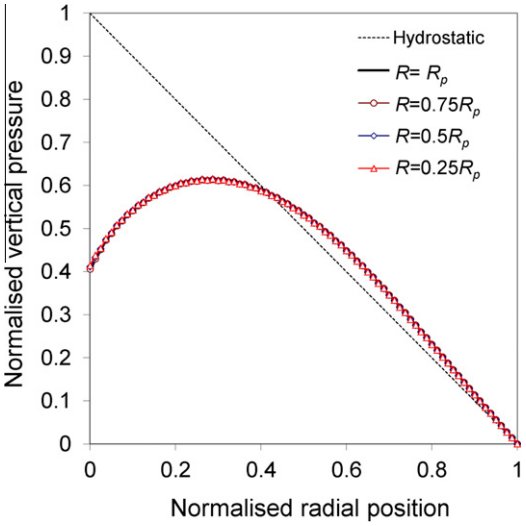

Fig. 9. Vertical base pressure distribution in piles with different sizes.

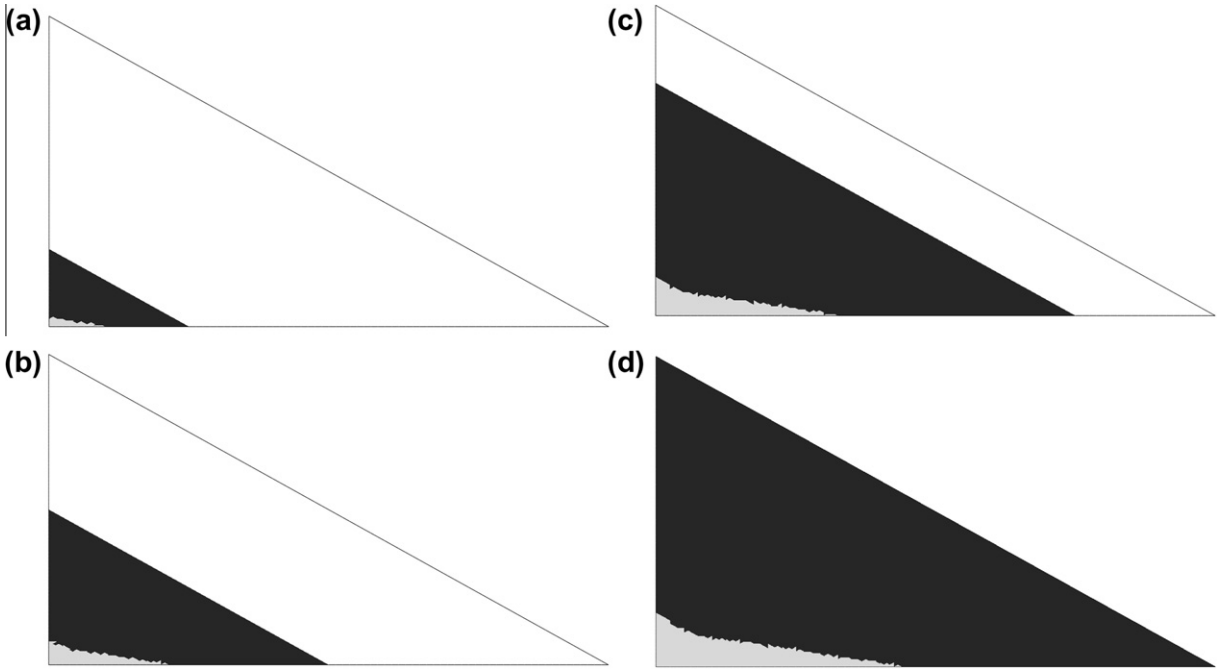

Fig. 10. Evolution of active plastic zone in a pile with $N_{el} = N_{cl} = 40$ (dark zone represents solid in plastic state). (a) after 10 layers; (b) after 20 layers; (c) after 30 layers; (d) after 40 layers.

The value of logarithmic bulk modulus κ can vary considerably for granular solids. Goodey et al. (2003) showed for a low stress level (up to 50 kPa), the κ value is rather small for stored solids (e.g., $\kappa = 0.002$ for Leighton Buzzard sand and $\kappa = 0.0025$ for pea gravel). In sandpile investigated in this study, the stress level is no higher than 5 kPa, so $\kappa = 0.002$ was chosen as the reference value. The void ratio of the granular solids typically ranges from 0.5 to 1.5. The initial void ratio was assumed to be $e_0 = 1$ in this study. The effects of these three parameters are investigated in a parametric study later in this paper.

2.4.3. Mohr–Coulomb plastic model and parameters

The Mohr–Coulomb (MC) yield function F_{mc} can be written as

$$F_{mc} = R_{mc} q - p \tan\phi - c = 0 \tag{5}$$

in which

$$R_{mc} = \frac{1}{\sqrt{3}\cos\phi} \sin\left(\Theta + \frac{\pi}{3}\right) + \frac{1}{3}\cos\left(\Theta + \frac{\pi}{3}\right)\tan\phi \tag{6}$$

where $R_{mc}(\Theta, \phi)$ is a measure of the shape of the yield surface in the deviatoric plane and Θ is the deviatoric polar angle; q is the Mises equivalent stress; Φ is the slope of the yield surface in the p–$R_{mc}q$ stress plane and is commonly referred to as the internal friction angle of the material; and c is the cohesion of the material. The MC flow potential G_{mc} adopted in Abaqus is a hyperbolic function in the meridional stress plane and the smooth elliptic function

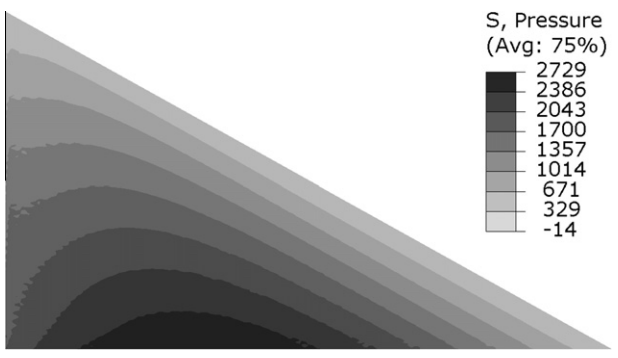

Fig. 11. Equivalent pressure stress p distribution (Unit: Pa).

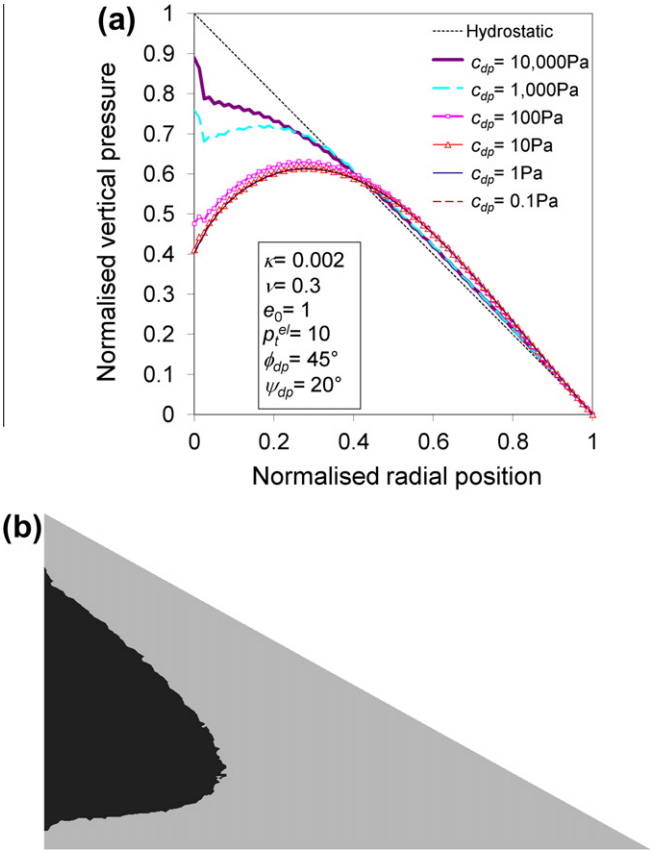

Fig. 12. Effect of cohesion c ($N_{el} = N_{cl} = 40$). (a) vertical base pressure; (b) predicted plastic zone with $c_{dp} = 1000$ Pa.

proposed by Menetrey and William (1995) in the deviatoric stress plane (see SIMULIA 2007).

Commonly the friction angle Φ is found to be very close to the repose angle α of the formed pile. A reference value was therefore chosen as $\Phi = \alpha = 29°$. A value of $\psi = 20°$ was chosen as the reference dilation angle. The real cohesion should be almost zero for dry cohesionless pellets, while in practice a nonzero cohesion parameter c (Eq. (5)) may be obtained from shear test results due to linear fitting of a curved failure surface. A very small reference value $c = 1$ Pa was chosen in this study, which is mainly to avoid numerical difficulties. The effects of these parameters are investigated in the next section.

2.4.4. Drucker–Prager plastic model and parameters

The Drucker–Prager (DP) yield function F_{dp} is given below:

$$F_{dp} = q - p\tan\phi_{dp} - c_{dp} = 0 \tag{7}$$

where Φ_{dp} is the slope of the yield surface in the p–q stress plane and is here referred to as the DP friction angle; c_{dp} is referred as the DP cohesion.

In the present study, the DP parameters are not directly available from experiments. However, the DP yield surface can be matched to the MC yield surface under specific loading conditions, as first suggested by Drucker and Prager (1952). Such a match can be represented by the coincidence points that two yield surfaces have in the deviatoric plane (as shown in Fig. 4). The relationships between these two sets of parameters from MC and DP models can be found as:

$$\tan\phi_{dp} = \frac{\tan\phi}{R_{mc}}, \qquad \frac{c_{dp}}{c} = \frac{1}{R_{mc}} \tag{8a, b}$$

The above equations are dependent on the value of angle Θ. Therefore, by choosing different value of angle Θ, the matched values between the two models are different, and the two yield surfaces would have different coincidence points in the deviatoric plane. Fig. 4 shows two extreme cases: one with the DP circle coinciding with the external apices of the MC hexagon and the other inscribing to the MC hexagon. The former corresponds to a tri-axial compression condition while the latter corresponds to a plane strain condition with associated flow (Drucker and Prager 1952). As confined by the two extreme cases, in a full range of Θ, the following relationships can be found:

$$\frac{3\sin\phi}{\sqrt{3+\sin^2\phi}} \leqslant \tan\phi_{dp} \leqslant \frac{6\sin\phi}{3-\sin\phi},$$
$$\frac{3\cos\phi}{\sqrt{3+\sin^2\phi}} \leqslant \frac{c_{dp}}{c} \leqslant \frac{6\cos\phi}{3-\sin\phi} \tag{9a, b}$$

For $\Phi = 29°$ and $c = 0$, Eq. (9) yields $\Phi_{dp} = 39 \sim 49°$ and $c_{dp} = 0$. The exact match for an axisymmetric loading condition as required in current axisymmetric sandpile modelling is not available. An empirical relationship drawn from a parametric study of the axisymmetic footing problem was given by Zimmermann et al. (2009) as

$$\tan\phi_{dp} = \frac{18\sin\phi}{9-\sin^2\phi}, \qquad \frac{c_{dp}}{c} = \frac{54\cos\phi}{9-\sin^2\phi} \tag{10a, b}$$

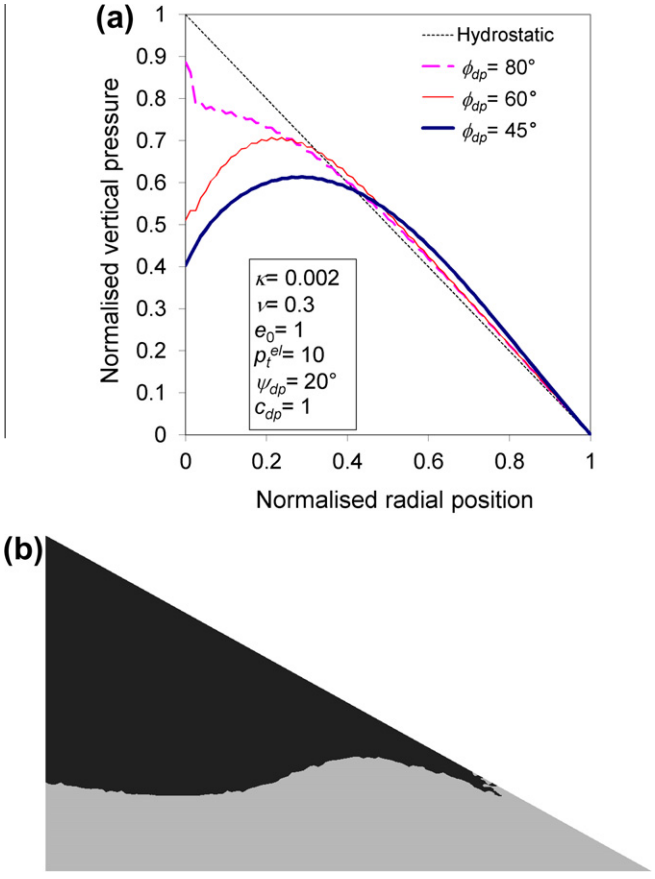

Fig. 13. Effect of friction angle Φ_{dp} ($N_{el} = N_{cl} = 40$). (a) vertical base pressure; (b) predicted plastic zone with $\Phi_{dp} = 60°$.

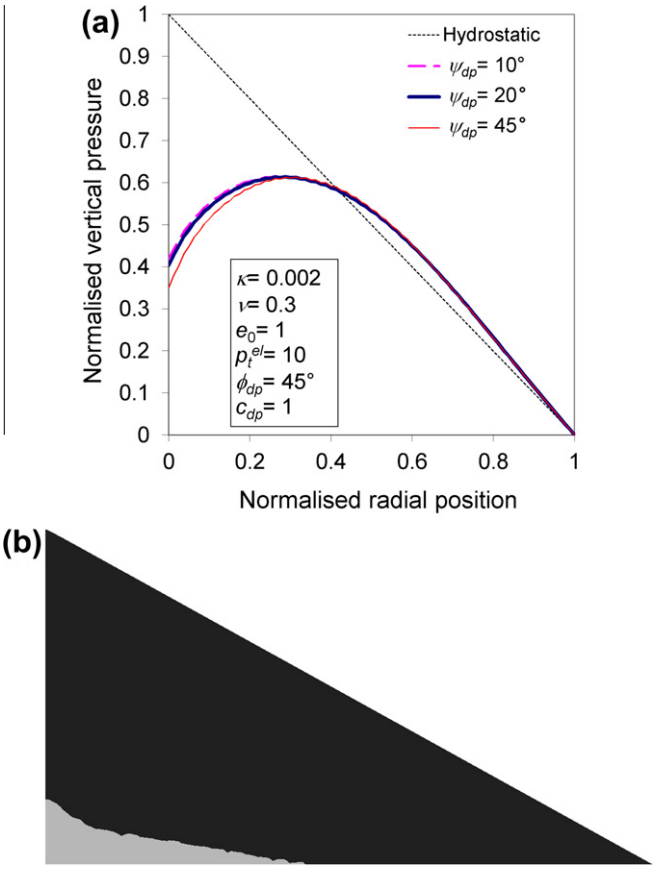

Fig. 14. Effect of dilation angle ψ_{dp} ($N_{el} = N_{cl} = 40$). (a) vertical base pressure; (b) predicted plastic zone with $\psi_{dp} = 45°$.

which give $\Phi_{dp} = 45^\circ$ and $c_{dp} = 0$ when $\Phi = 29^\circ$ and $c = 0$. These matched values provide a basis on which the effect of the MC and DP models on predicted sandpile behaviour can be approximately compared. It may be appreciated that the sandpile model with DP friction angle smaller than 45° is likely to be physically

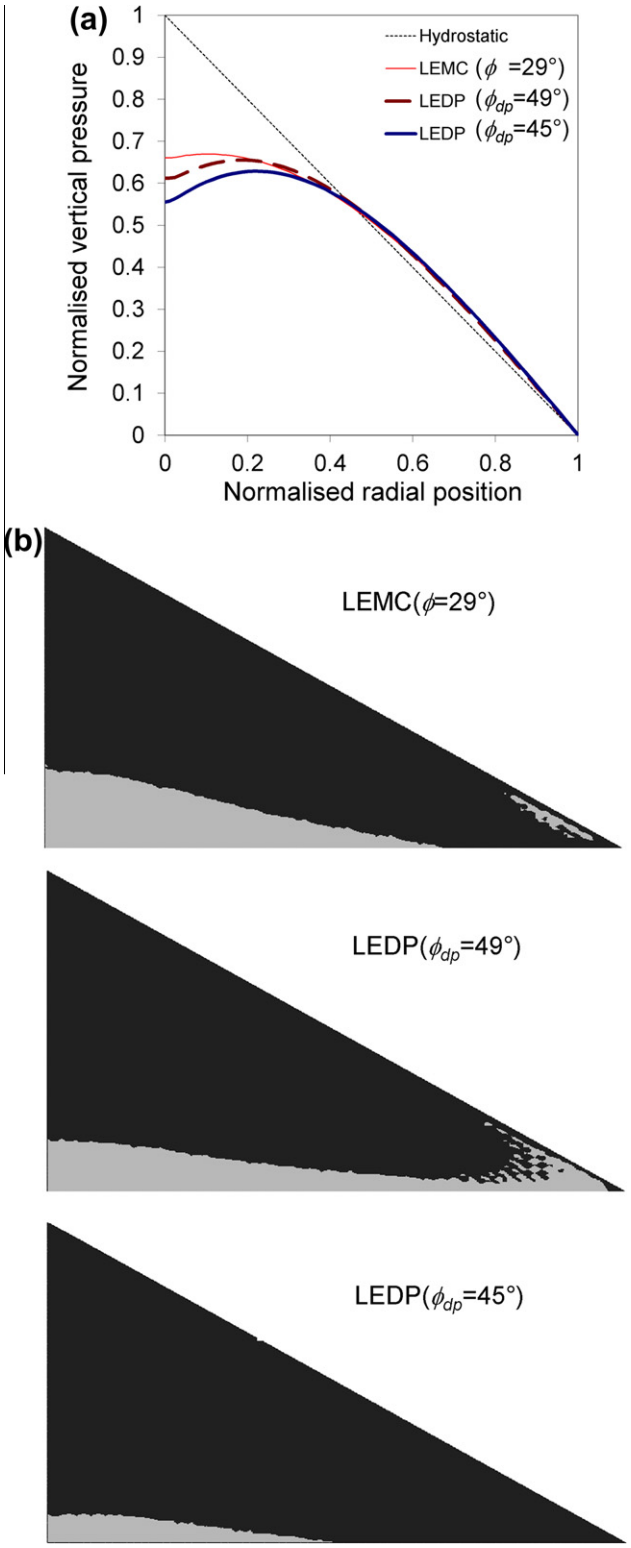

Fig. 15. Comparisons of predictions of the MC and DP models. (a) base pressure distribution; (b) plastic zone at the completion of the piles.

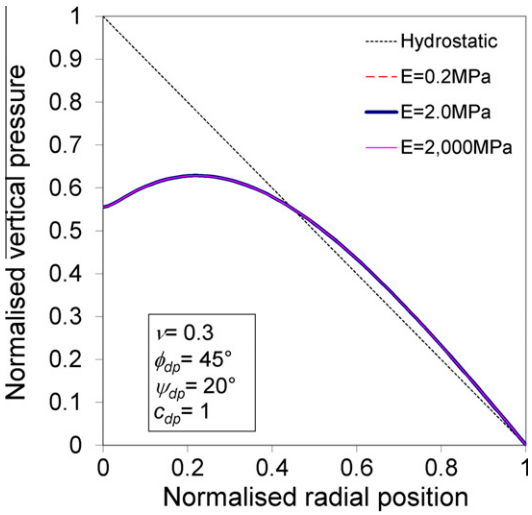

Fig. 16. Effect of linear elastic modulus on the base pressure distribution (LEDP model).

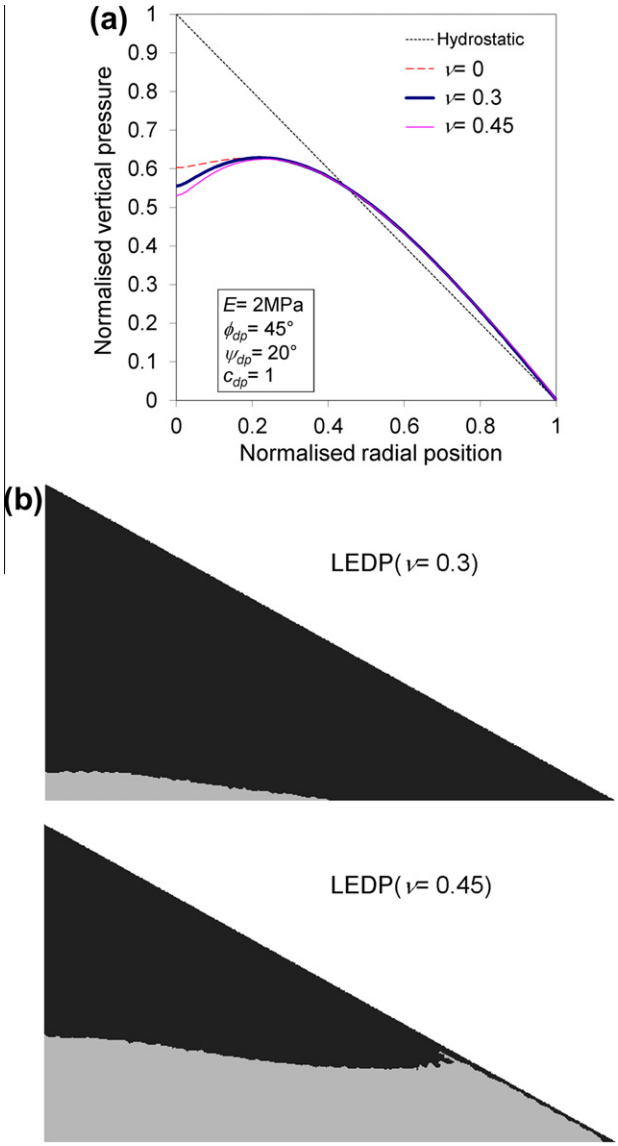

Fig. 17. Effect of Poisson's ratio on base pressure distribution (LEDP model). (a) vertical base pressure; (b) predicted plastic zones.

unstable under gravity, because sandpile is unstable with $\Phi < \alpha$. In this study, the DP friction angle and DP dilation angle were chosen as 45° and 20°, respectively.

All the parameters adopted in the FE calculations for the reference case are summarised in Table 1.

3. Results and discussions

3.1. Effect of constitutive models

3.1.1. Results based on the "switched-on" construction

The predicted base pressure distributions underneath the sandpile at the final stage for different constitutive laws using the switched-on gravity loading procedure is compared with experimental observation in Fig. 5. The pressure was normalised using the hydrostatic pressure under the apex at the base $p = \gamma H_p$ where γ is the bulk density and H_p is the height of the pile. Fig. 5a shows that all five elastic and elastic–plastic models predicted the maximum vertical pressure to be at the centre, which concur with the results of Savage (1998) FEM calculations. The base pressure is lower than the hydrostatic value towards the centre and slightly higher than the hydrostatic value elsewhere, satisfying the global equilibrium in the vertical direction. However, different models predicted different values of the maximum vertical pressure, indicating that different amounts of the weight are deflected away from the centre. Compared with the LE elastic model, the PE elastic model predicted a higher value of the central vertical pressure, while the three elastic–plastic models all predicted lower values indicating that plasticity has resulted in a greater distribution of the central loads radially outwards.

Michalowski and Park (2004) proposed an internal arching mechanism in a pile, such that the vertical base pressure distribution cannot follow the shape of the pile in order to satisfy both force and moment equilibrium of the pile body. This implies that no pile with cohesionless solids can be obtained in an ideally frictionless flat base, except in extreme cases such as that the particles are aligned in vertical columns with no horizontal interaction. In contrast, a larger base shear force may facilitate a larger arching effect, resulting in the resultant vertical reaction force being further away from resultant gravitational force.

The predicted base shear traction distributions shown in Fig. 5b support this proposition. Compared with the LE model, the PE model produced comparable magnitude of maximum base shear traction that occurred at a smaller radial position, resulting in a smaller total shear force. The LEMC, LEDP and PEDP models all produced larger shear tractions than the LE and PE elastic models that gave a larger arching effect and resulted in smaller central base pressures.

3.1.2. Results based on the progressive mesh activation scheme

Next, the predicted base pressure distributions for different constitutive laws using progressive mesh activation procedure with $N_{cl} = 40$ construction layers are shown in Fig. 6. The two elastic LE and PE models both predicted highest vertical pressure at the centre, while a central dip in vertical pressure was predicted by all of the elastic–plastic models. The predicted shear tractions were much larger than in the switched-on procedure for the elastic–plastic models, amongst which the PEDP model produced the largest dip and the LEMC model produced the smallest dip. It is noted that the rate of increase of shear traction from the centre as

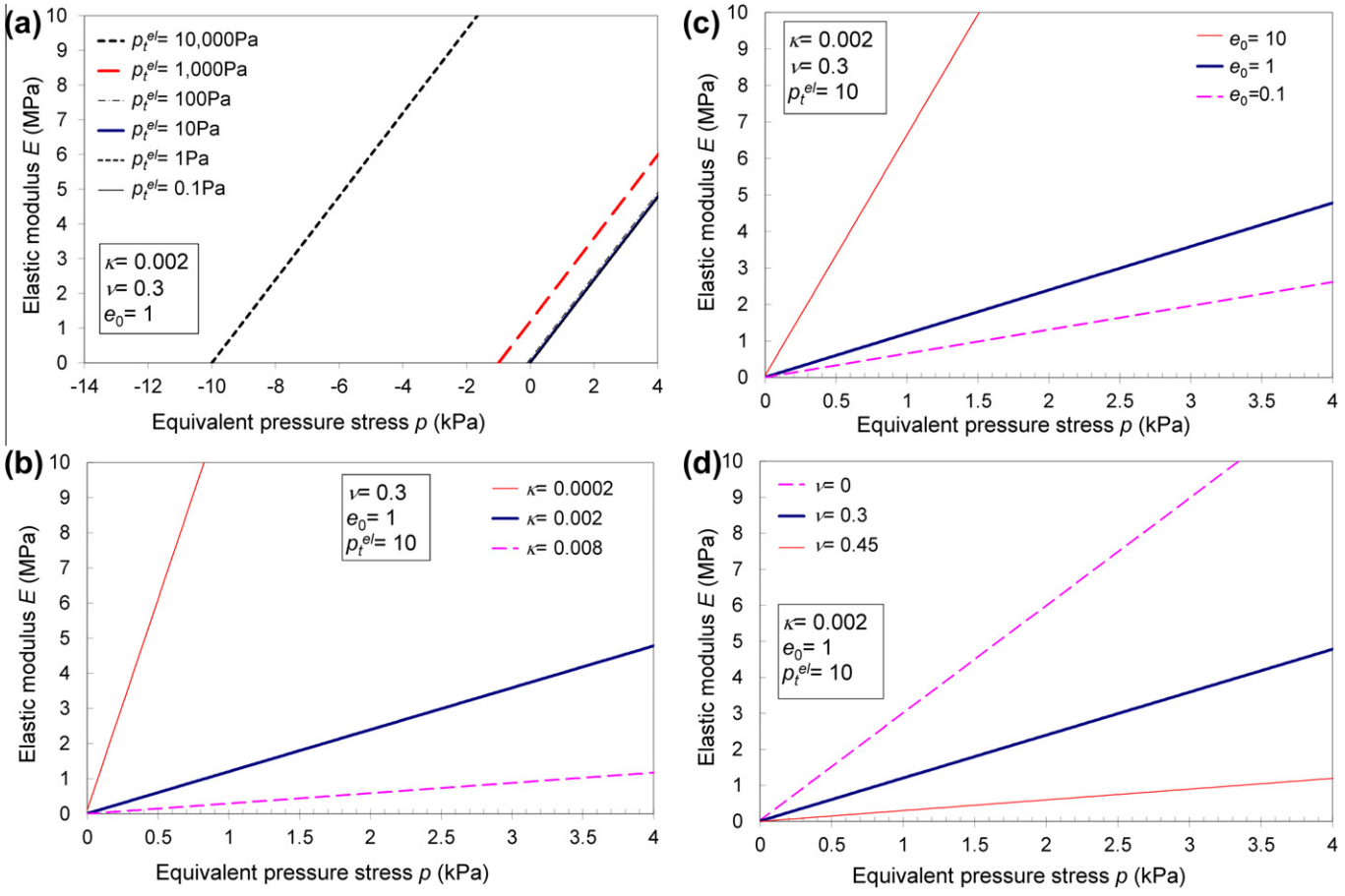

Fig. 18. Effect of p_t^{el}, κ, e_0 and ν on the porous elastic model behaviour p–E.

represented by the initial slope of the shear traction curves is important in relation to the size of predicted dip. As shown in Fig. 6b, a larger initial slope corresponds to a larger extent of central vertical pressure suppression. The slope of the shear traction curve at the centre is largest for the PEDP model and smallest for LEMC model. For all the computations presented in both Fig. 5 and Fig. 6, the mobilised friction coefficient on the base (ratio of shear traction to vertical pressure) was well below 0.4, confirming the fully rough base assumption made in the calculations is valid.

The comparison between Fig. 5 and Fig. 6 shows that the effect of progressive mesh activation procedure appears to be different when elastic or elastic–plastic models is used. The results also support the proposition that material plasticity is important for predicting the sandpile phenomenon. In addition, the stress-dependency of the elastic modulus appears to be able to significantly enhance the pressure dip. Since all numerical predictions so far still under-predicted the magnitude of the central pressure dip, this factor may provide a further insight into the phenomenon and will be explored further.

3.1.3. Effect of number of construction layers

Based on the understanding of the benchmark test illustrated above, the effect of number of construction layers on sandpile modelling was explored. The result using PEDP (porous elastic with Drucker–Prager plasticity) model with parameters listed in Table 1 (except $\Phi_{dp} = 50°$) is shown in Fig. 7. It is shown that all cases predicted a central pressure dip except the switched-on gravity case ($N_{cl} = 1$) which predicted the maximum pressure at the centre. The result also shows that the greater the number of construction layers used, the larger was the size of the dip predicted. This result indicates that the numerical process of layer construction significantly affects the prediction. This suggests that modelling the progressive loading history during sandpile formation may be vital in numerical modelling of sandpile. Since the modelled pile had a height of around 0.3 m and the mean particle diameter of 3 mm, the maximum number of layer won't exceed 100 if the thickness of one layer is assumed as equal to the mean particle diameter. The relationship between layer thickness and predicted pressure dip is given in the inset of Fig. 7 for the range of $N_{cl} = 1 \sim 80$. The results suggest that very large number of layers would be required to predict the pressure profile more accurately.

3.2. Evolution of stress distribution and plastic zone during sandpile formation

Since the porous elastic with Drucker–Prager plasticity PEDP model produced the largest dip and closest prediction to the experimental data, the PEDP model with progressive mesh activation scheme is used in the rest of the paper to further investigate the sandpile behaviour.

Major questions on sandpile behaviour during formation include: (1) whether the pressure dip is localised at the bottom boundary or if it propagates up to the apex of the pile; (2) whether the pressure dip develops from the beginning of the formation, and its size increases during the pile formation process; (3) how does the plastic zones distribute within the solid and evolve during the formation process. Fig. 13–15 show the main FEM results using

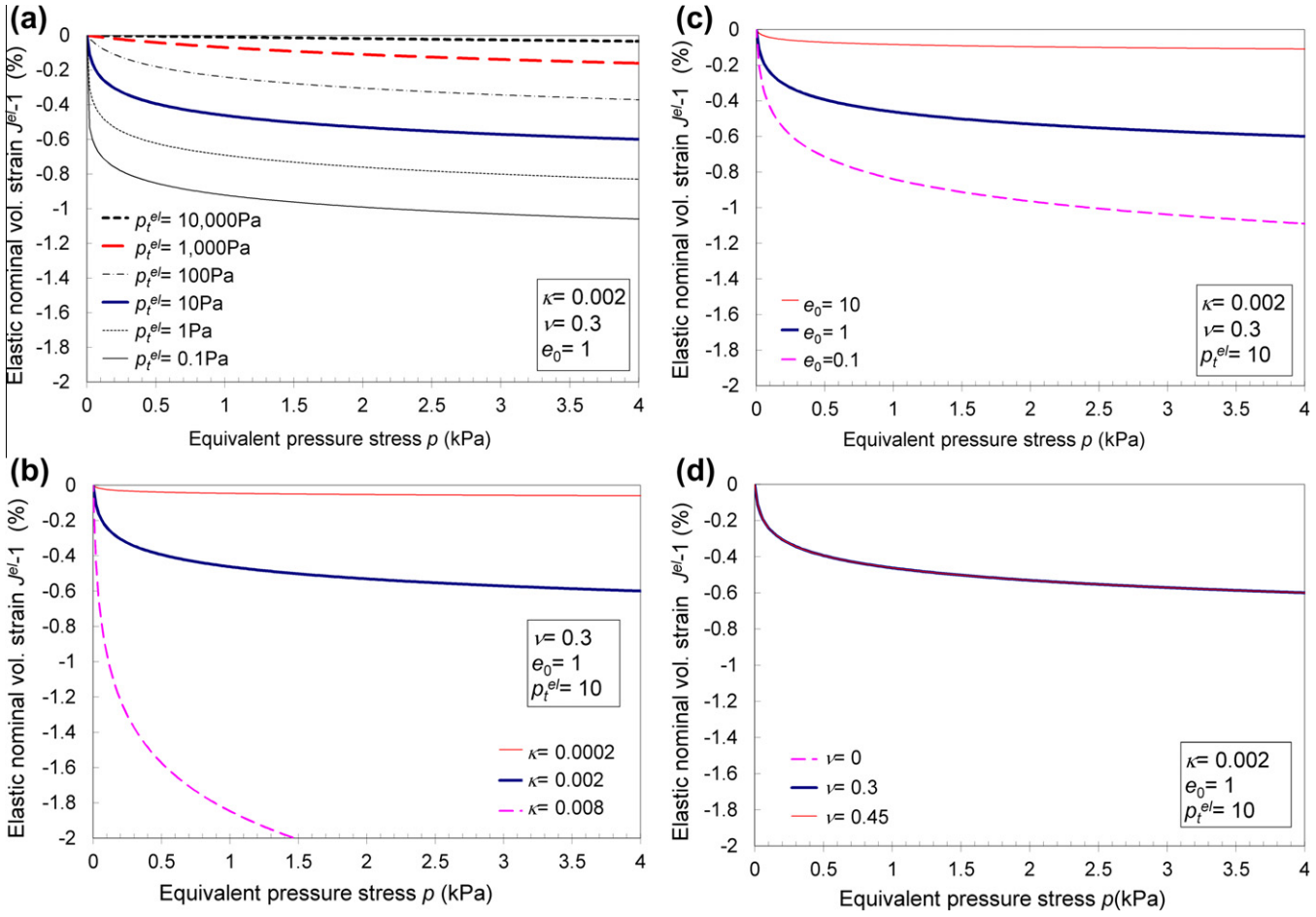

Fig. 19. Effect of p_t^{el}, κ, e_0 and ν on the porous elastic model behaviour p–$J^{el} - 1$.

the PEDP model and progressive mesh activation procedure with 40 layers of elements and construction layers ($N_{cl} = N_{el} = 40$).

Most of the earlier experiments only measured the base pressures, so the stress distributions inside the pile were unknown. By using the photoelastic technique, some studies (Geng et al. 2001; Zuriguel and Mullin 2008) have obtained the stress field within two dimensional piles, showing that the pressure dip exists not only at the bottom boundary but also inside the pile at all levels. The present FEM study concurs with this observation as can be seen from the contour of the predicted vertical stress σ_v in Fig. 8a and the vertical stress along the horizontal paths at different heights after pile construction in Fig. 8b. The pressure dip propagated up to the top with the dip size decreasing from the base upwards.

Fig. 9 compares the vertical base pressure distribution from four piles with radius of $R = 0.25R_p$, $0.5R_p$, $0.75R_p$ and R_p, representing different stages of the formation process. In order to eliminate the effect of mesh density and layer density (c.f. Fig. 7), all the four pile models had the same number of construction layers and elements. Fig. 9 shows clearly that the normalised pressure dip is predicted to be independent of the pile size. This suggests the pressure dip develops from the beginning of the pile formation and its relative size remains the same during the whole progressive formation process. The validity of this observation lies in the fact that the simulation was treated as static, so the solid deposition rate and impact energy were not considered. The solid deposition rate and impact energy can affect the resultant pressure distribution: this requires further investigation and is beyond the scope of this study. Another important factor is that the finite size of the deposition stream was ignored in the simulation. In reality, the size of deposition stream would be relatively large compared to the transient pile size when the pile is small. Experimental studies have suggested that the relative deposition size has a significant effect on the dip formation (Vanel et al. 1999; Geng et al. 2001; Ai 2010).

The evolution of plastic zone during pile formation is illustrated in Fig. 10. The elastic and plastic zones are represented by light and dark grey areas respectively. The FEM computation predicted a small elastic inner core surrounded by large zones in the yielding state. Such a pattern has some similarity to some earlier solutions of admissible stress field that contain a pressure dip (e.g., Didwania et al. 2000; Michalowski and Park 2004). The patterns of the elastic and plastic zones were similar at different loading stages. Note that part of the plastic zone at an earlier layering stage might become elastic at a later stage. This phenomenon indicates that the material was in a plastic state when it was newly layered on the existing pile, and part of it became elastic due to an increase of confining stress when subsequent layers were added.

Fig. 11 shows the distribution of the equivalent pressure stress p within the pile. Because the instantaneous elastic modulus is dependent on the value of p according to Eq. (4), the variation of the elastic stiffness in this model is directly related to the distribu-

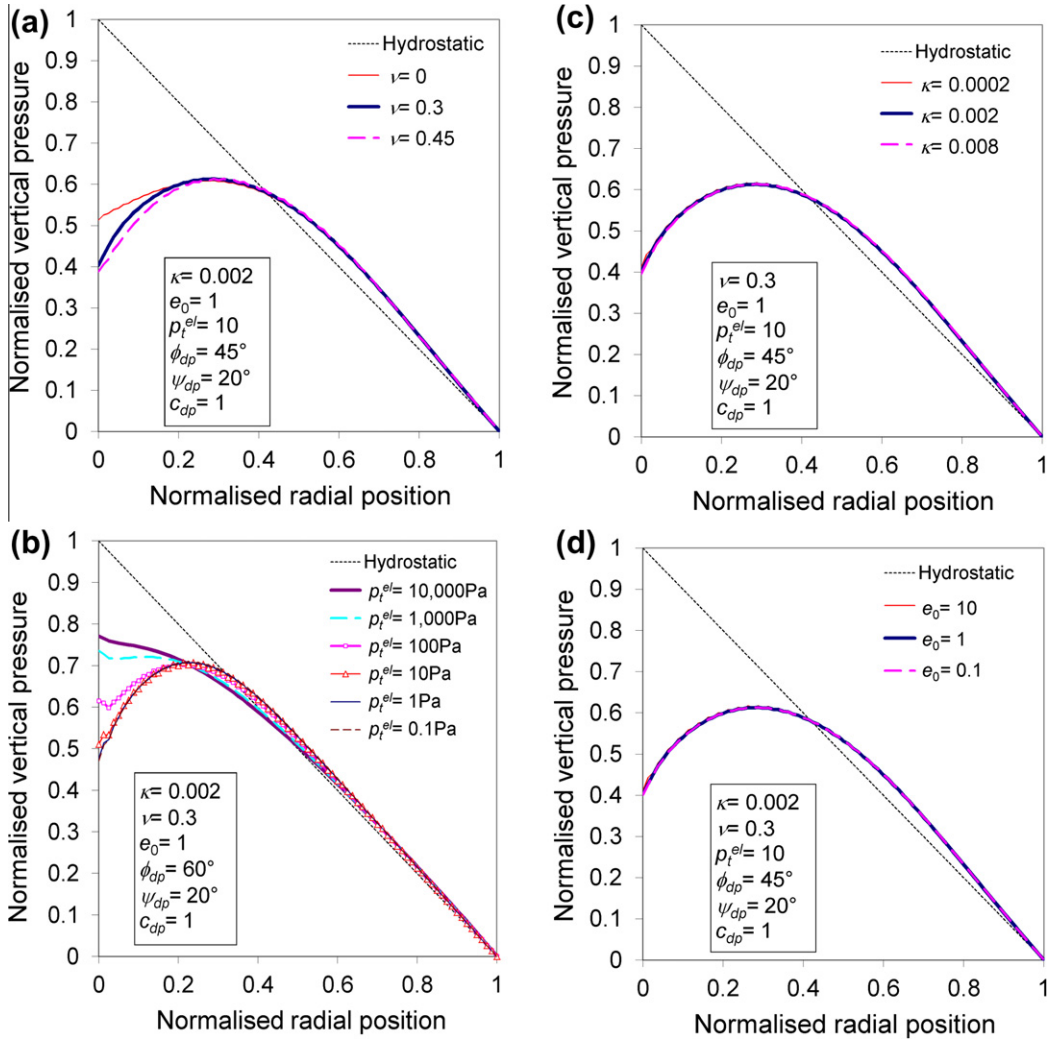

Fig. 20. Effect of porous elastic parameters on the pressure dip prediction. (a) ν; (b) p_t^{el}; (c) κ; (d) e_0.

tion of p, with the stiffness increasing when p increases. The elastic stiffness generally increases with depth at a given radial position. The largest elastic stiffness at each height level is some radial distance away from the centre, giving rise to an elastically softer central core surrounded by a stiffer region if the contribution from plasticity is ignored. Although most of the solid in the pile was predicted to yield plastically at some stage during the formation process, the elastic stiffness would still be affecting the initial plastic flow. This may be one of the reasons for the larger pressure dip predicted by the PEDP model than that by the LEDP model where the elastic modulus is constant everywhere (Fig. 6a).

3.3. Effect of plastic parameters

Plastic failure appears to play an important role in producing the pressure dip as has been shown in Fig. 6. It is therefore necessary to explore the effects of the plastic parameters on the prediction. Fig. 12 shows the predicted base pressure distribution with different values of cohesion c. In the reference case, the cohesion was chosen as a very small value $c_{dp} = 1$ Pa to represent the cohesionless solid. It is clear from Fig. 12a this treatment is valid since the predicted pressure distribution remained essentially the same when c_{dp} is smaller than 10 Pa. As c_{dp} increased further, more solid behaved elastically which resulted in a smaller pressure dip. If c_{dp} is very large (e.g. $c_{dp} = 10$ kPa), all the solid became elastic so the solution reduced to purely elastic prediction as no plastic failure is possible. It is evident that the curve with $c_{dp} = 10{,}000$ Pa in Fig. 12 is the same as that predicted by the purely elastic PE model in Fig. 6a. With a value of cohesion $c_{dp} = 1$ kPa the plastic zone was confined to the middle of the pile (Fig. 12b), as which is not realistic one would expect the free surface to be in a yield condition.

Fig. 13a shows the effect of friction angle Φ_{dp}. An increase of the friction angle results in smaller pressure dip and higher maximum vertical pressure. Fig. 13b shows the plastic zone predicted with $\Phi_{dp} = 60^\circ$, where the size of the plastic zone decreased and occupied only the upper part of the pile, compared with the reference case of $\Phi_{dp} = 45^\circ$ (Fig. 10d). No converged solution was achieved with values of Φ_{dp} smaller than 45°. As suggested in previous section, the pile would not be physically stable with $\Phi < \alpha$, so no stable static solution may be obtained.

Jeong and Moore (2010) found the effect of dilation angle to be negligible in his computations. This study found dilation angle to have a noticeable though limited effect on the prediction. Fig. 14a shows that a larger dilation angle resulted in a slightly larger pressure dip, but it has little effect on the plastic zone (Fig. 14b). The dilation angle controls the plastic volume change during shear failure, and a larger dilation angle leads to a larger increase in volume during plastic state. The radial component of this volume increase would promote a larger base traction, which produces a larger arching effect and thus a larger pressure dip.

It is also of interest to compare the predictions from the Mohr–Coulomb model and the Drucker–Prager model. As suggested in the previous section, the comparison of these two models has to be based on a comparable MC friction angle Φ and a DP friction angle Φ_{dp}. Eq. (9) gives the comparable value of the DP friction angle in range of $\Phi_{dp} = 39^\circ \sim 49^\circ$ for a MC friction angle of $\Phi = 29^\circ$. Fig. 6a has shown that the LEMC model with $\Phi = 29^\circ$ predicted a smaller pressure dip than the LEDP model with $\Phi_{dp} = 45^\circ$. Fig. 15a further shows the LEDP model with $\Phi_{dp} = 49^\circ$ still predicted a larger dip than the LEMC model with $\Phi = 29^\circ$. No converged solution was obtained for friction angles smaller than $\Phi = 29^\circ$ for the MC model and $\Phi_{dp} = 45^\circ$ for the LEDP model as the solid is at a physically instable configuration. The pattern of the plastic zone predicted by the LEMC model is slightly different from those predicted by the DP model (Fig. 15). It may thus be concluded that for the same failure properties, the DP model predicted a larger pressure dip than the MC model. Nevertheless, further investigation is still needed to fully understand this phenomenon.

3.4. Effect of elastic parameters

Fig. 16 shows the almost identical predictions using the LEDP model with different value of elastic modulus E ranging from 0.2 MPa to 2000 MPa. This is consistent with the conclusion of some previous calculations in silos (e.g., Ooi and Rotter 1990; Goodey et al. 2003; Goodey et al. 2006) where the stress distribution is not sensitive to the magnitude of the elastic modulus.

The second elastic parameter, the Poisson's ratio, shows a significant effect on the pressure dip prediction. A larger Poisson's ratio results in a large pressure dip (Fig. 17a). It may be noted that in the calculations by Jeong and Moore (2010) where a dip size as large as in experiment was predicted, a large value of Poisson's ratio $\nu = 0.45$ was adopted. As the Poisson's ratio controls the elastic strain of the pile in the horizontal direction when the pile is loaded in vertical direction, a larger Poisson's ratio would naturally increase the lateral elastic expansion. This lateral expansion tends to generate a larger base traction which in turn results in an enhanced arching effect. The effect of an increase of the Poisson's ratio and the dilation angle is similar: increasing the radial expansion respectively in the elastic and plastic part. The size of plastic zone was predicted to reduce with an increase of the Poisson's ratio and the larger pressure dip (Fig. 17b). This effect is in contrast to the effect of plastic parameters where a larger plastic zone corresponded to a larger pressure dip.

The porous elastic stress-dependent modulus has been shown in Fig. 6a to play a vital role in producing the largest pressure dip that has the closest match to the experiment. Here the effect of the porous elastic parameters is explored. Among the five input parameters in the porous elastic model in Abaqus (Logarithmic bulk modulus κ, initial equivalent pressure stress p_0, elastic tensile stress limit p_t^{el}, initial void ratio e_0 and Poisson's ratio ν), the value of p_0 was always set as zero, so did not feature in this parametric study. To better illustrate the effect of each parameter in the porous elastic model, the elastic modulus E and the elastic nominal volumetric strain $J^{el} - 1$ were evaluated against the equivalent pressure stress p, as shown in Figs. 18 and 19. It is shown that the p–E relationship (given by Eq. (4)) is almost linear in the range of p in this example pile. The equivalent elastic modulus E starts from zero at the negative value of p_t^{el} and may increase at different rates according to the various input parameters. The elastic nominal strain $J^{el} - 1$ develops similarly at different rate for all parameters, except for Poisson's ratio ν which doesn't affect the value of $J^{el} - 1$ according to Eq. (1).

The effect of the tensile stress limit p_t^{el} on the pressure dip prediction was explored using a DP friction angle $\Phi_{dp} = 60^\circ$ (Fig. 20b) and all other cases were explored using $\Phi_{dp} = 45^\circ$ (Fig. 20a, c and d). As shown in Fig. 20a, the effect of the Poisson's ratio in the prediction using PEDP is consistent to that using LEDP as described earlier (Fig. 17). Fig. 20c and d show that the logarithmic bulk modulus and initial void ratio have almost no influence in the large practical range explored. This suggests that the increasing rate of the instantaneous elastic modulus E with the equivalent pressure stress p is not important in producing the pressure dip. However, the value of the tensile stress limit p_t^{el} has a very significant effect on the prediction (Fig. 20b). The effective range of modulus E (Fig. 18) is confined to the range with positive p. As a result, the value of p_t^{el} determines the starting value of the instantaneous elastic modulus E (Fig. 18) in the pile calculation: a large input value of p_t^{el} resulted in a large starting value of E. Fig. 20b shows that when the value of p_t^{el} increased the size of the predicted pressure dip decreased and finally disappeared when p_t^{el} increased beyond the maximum tensile stress in the pile. In the other direction, as the value of p_t^{el} approached zero, the prediction converged. This behaviour suggests the magnitude of the initial value of the elastic modulus has an important influence in the

prediction. It indicates that methods adopting a constant elastic modulus (e.g. LEMC, LEDP) are not capable of capturing this important stress-dependent characteristic of granular solids.

4. Concluding remarks

This paper has presented an investigation into the pressure dip phenomenon using the finite element (FE) method. The effects of factors including the progressive mesh activation, stress-dependent elastic modulus and plastic failure parameters have been explored by modelling a conical sandpile adopting five relatively simple elastic and elasto-plastic constitutive models.

The results have shown that significant pressure dip can be predicted without incorporating material anisotropy. However, no pressure dip can be predicted without considering the progressive mesh activation process or plasticity. Significantly smaller pressure dip than observed in experiments is predicted when using a linear elasto-plastic model incorporating progressive mesh activation process. The inclusion of stress-hardening elasticity is important in significantly enhancing the dip, to the extent in close agreement with experimental observations. A similarity of the plastic zone pattern has also been observed between the FE predictions and earlier limit analysis solutions. The effects of the elastic and plastic parameters have been explored. Apart from the internal friction angle, the results have suggested that the Poisson's ratio and the dilation angle have some effects on the size of the pressure dip. The results have shown a strong relationship between the development of base shear, internal arching and pressure dip.

Acknowledgements

We acknowledge the support from the EPSRC (grant GR/T23541) and the Scottish Funding Council for the Joint Research Institute with the Heriot-Watt University which is a part of the Edinburgh Research Partnership in Engineering and Mathematics (ERPem). J.A. also acknowledges the support from an Edinburgh University Research Scholarship and further support from the EPSRC (grant EP/H011951/1) for his work at Nottingham University after completing his PhD. The authors are very grateful to Prof. J.M. Rotter and Prof. H.S. Yu for their many helpful discussions on this topic.

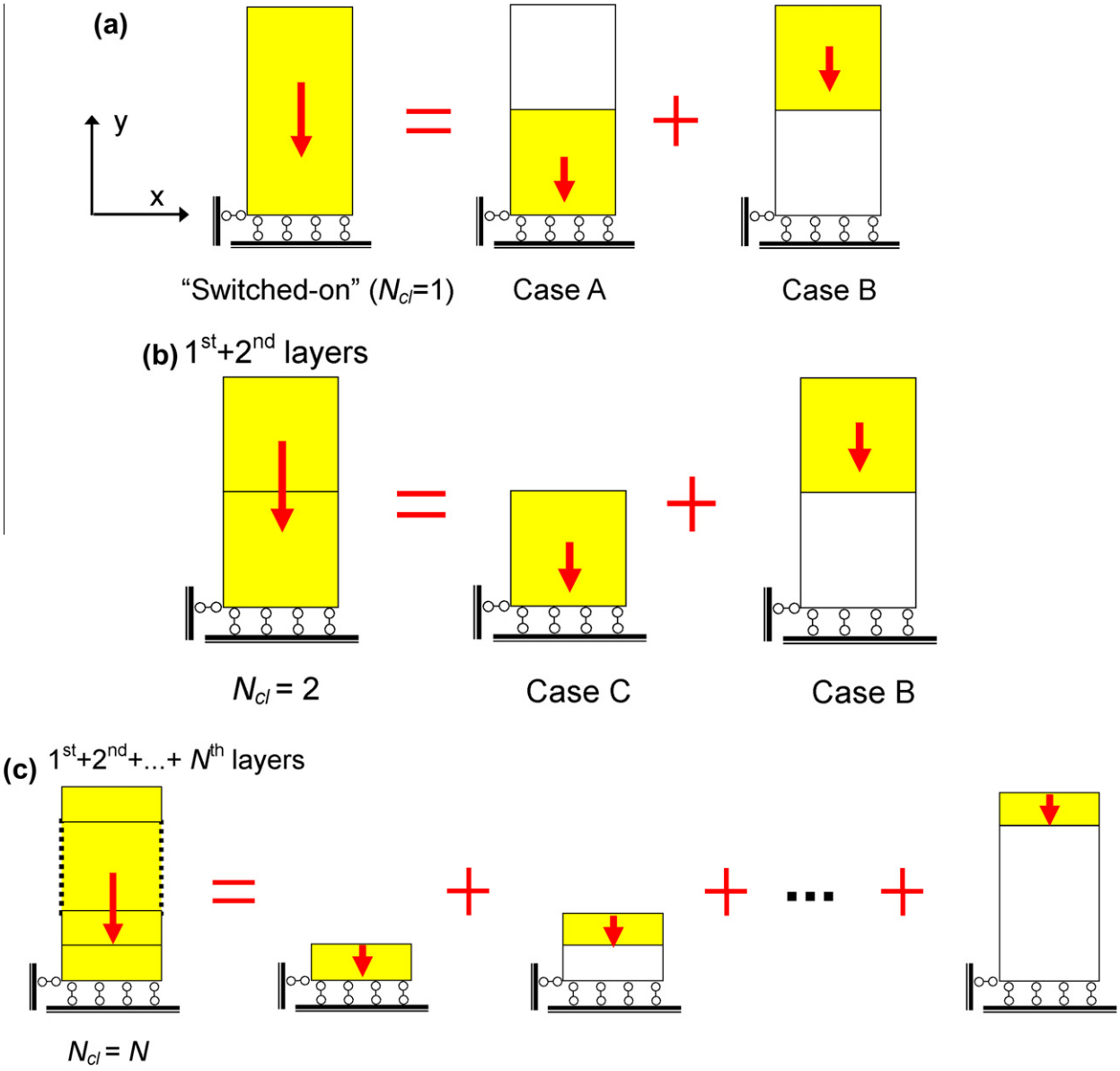

Fig. A1. Effect of progressive mesh activation. (a) Switched-on gravity loading; (b) progressive mesh activation with two construction layers; c) progressive mesh activation with N construction layers. The shaded parts have both stiffness and self-weight activated; the blank parts only have stiffness activated but not self-weight.

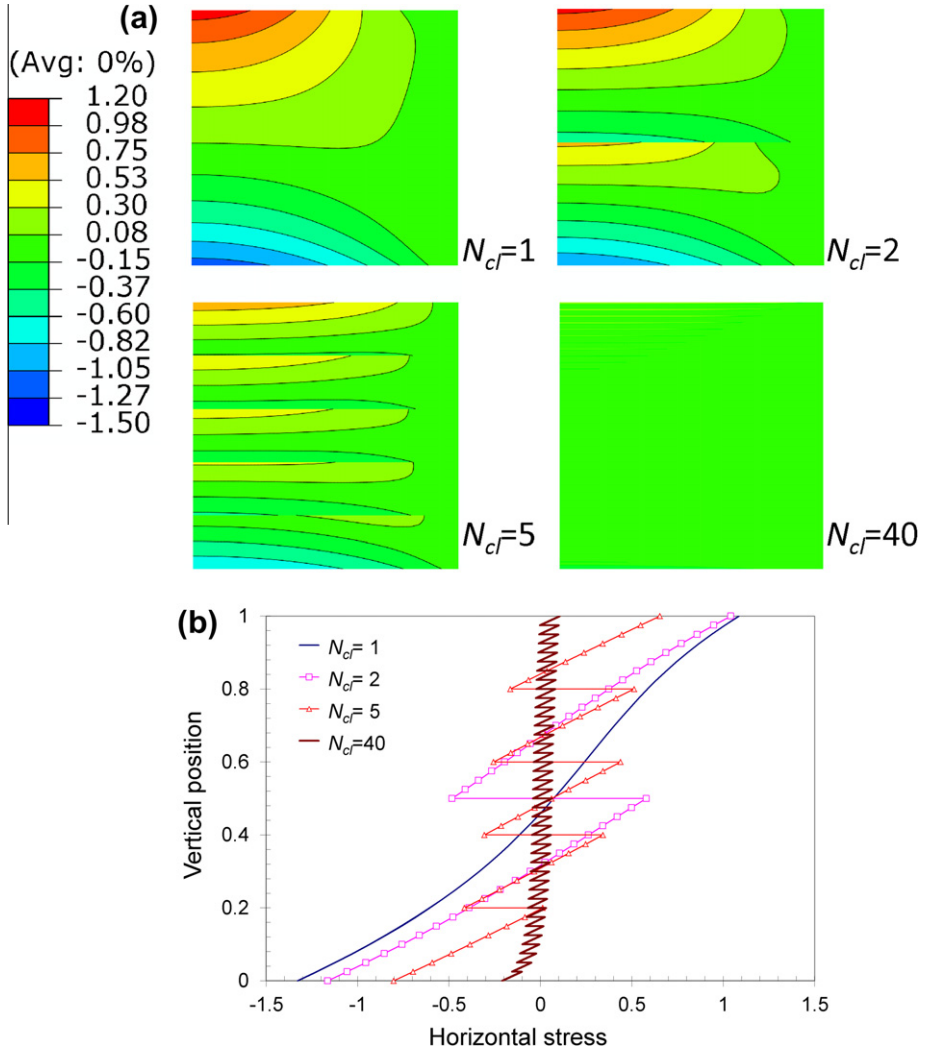

Fig. A2. Effect of number of layers on the stress distribution for an elastic model. (a) Contour of horizontal stress in the elastic body (only right half is shown); (b) horizontal stress along the central axis of symmetry. The vertical coordinate is normalised by the model height L_v and the stress magnitude is normalised by 0.1 $\rho g L_v$.

Appendix A. Benchmark test of progressive mesh activation

The effect of progressive mesh activation on the behaviour of structures under self-weight may be illustrated by a simple example as shown in Fig. A1. The model consists of a rectangular body supported on a frictionless rigid surface and settles under gravity. For simplicity and without the loss of generality, the system is assumed to be both geometrically and materially linear.

When the rectangular body deforms under switched-on gravity loading (the leftmost case in Fig. A1a), it can be proven that unless the Poisson's ratio equals to zero there exist in the body non-zero shear stresses τ_{xy} as well as horizontal stresses σ_x which are tensile in the upper part and compressive in the lower part of the body, in additional to vertical stresses. Because the system is linear elastic, the "switched-on" case can be decomposed into Cases A and B with boundary conditions identical to their parent case, except that the gravity is only activated in the lower or the upper half respectively (Fig. A1a). The stress field of the "switched on" case is equivalent to the superposition of those of Case A and Case B.

The situation is different for progressive mesh activation. As shown in Fig. A1b, when the rectangular body is constructed in two stages (leftmost case in Fig. A1b), it should instead be decomposed into Cases C and B, where Case C has both the stiffness and loading of the upper half deactivated. Similarly, the decomposition of an N layer case is shown in Fig. A1c. It should be noted that the treatment of the stiffness activation for the newly added layer is very important in a progressive mesh activation scheme for modelling progressively formed structures.

For switched-on gravity loading, the deformation of the lower layer is restrained by the upper layer in Case A so there is no stress discontinuity. For the case of two-layer progressive mesh activation case, when the lower layer is constructed, its gravitational body force results in a tensile horizontal stress σ_x at the top and a compressive σ_x at the bottom of the lower layer. When the upper layer is added but before its body gravity is applied, the upper layer is stress free. This induces a stress discontinuity in σ_x at the boundary between the two layers. When the gravity is applied to the top layer, it results in a tensile σ_x at the top of the upper layer, but a compressive σ_x towards the bottom of the upper layer. This in turn induces a compressive σ_x in the lower layer which compensates some tensile σ_x at the top of the lower layer but the stress discontinuity between the two layers still exists. If the body is constructed with many more layers (leftmost case in Fig. A1c), both the value of σ_x and the extent of discontinuity between the layers are progressively reduced.

The phenomenon discussed above is confirmed by the numerical results shown in Fig. A2. An elastic body with a width of $L_h = 2.0$ m and height of $L_v = 1.0$ m was used to calculate the horizontal stress distribution, constructed with 1, 2, 5 and 40 layers. A density of $\rho = 1.0$ kg/m^3, elastic modulus of $E = 1.0$ MPa and Poisson's ratio of $\nu = 0.3$ were used in the calculations. Only the

right half of the body was modelled and discretised into 40×40 square 8-noded quadratic elements. It is shown that large gradient of horizontal stress is produced in the body if constructed by the "Switched-on" loading procedure, while almost uniform and zero-valued horizontal stress is produced by progressive layering procedure. In addition, the number of construction layers also plays an important role on the magnitude of the stress discontinuity at the interfaces between the layers.

References

Ai, J., 2010. Particle scale and bulk scale investigation of granular piles and silos, Ph.D. Thesis School of Engineering, The University of Edinburgh, Edinburgh, UK.

Ai, J., Chen, J.F., Rotter, J.M., Ooi, J.Y., 2009. Finite element prediction of progressively formed conical stockpiles. In: 2009 SIMULIA Customer Conference, London, U.K., pp. 375–387.

Al Hattamleh, O., Muhunthan, B., Zbib, H.M., 2005. Stress distribution in granular heaps using multi-slip formulation. Int. J. Numer. Anal. Meth. Geomech. 29 (7), 713–727.

Anand, L., Gu, C., 2000. Granular materials: constitutive equations and strain localization. J. Mech. Phys. Solids 48 (8), 1701–1733.

Atman, A.P.F., Brunet, P., Geng, J., Reydellet, G., Claudin, P., Behringer, R.P., Clément, E., 2005. From the stress response function (back) to the sand pile 'dip'. Eur. Phys. J. E 17 (1), 93–100.

Aubry, D., Hujeux, J.C., Lassoudie're, F., Meimon, Y., 1982. A double memory model with multiple mechanisms for cyclic soil behaviours. In: Int. Symp. Nu. Models in Geomechanics, Zurich, pp. 3–13.

Cates, M.E., Wittmer, J.P., Bouchaud, J.P., Claudin, P., 1998. Development of stresses in cohesionless poured sand. Philos. Trans. Roy. Soc. A 1998 (1747), 2535–2560.

Chen, J., Yu, S., Ooi, J., Rotter, J., 2001. Finite-element modeling of filling pressures in a full-scale silo. J. Eng. Mech. ASCE 127 (10), 1058–1066.

Clough, W., Woodward, J., 1967. Analysis of embankment stresses and deformations. ASCE J. Soil Mech. and Found. Div. 93 (4), 529–549.

de Gennes, P.G., 1999. Granular matter: a tentative view. Rev. Mod. Phys. 71 (2), 374–382.

Didwania, A., Cantelaube, F., Goddard, J., 2000. Static multiplicity of stress states in granular heaps. Proc. Roy. Soc. A 456 (2003), 2569–2588.

Drucker, D., Prager, W., 1952. Soil mechanics and plastic analysis or limit design. Q. Appl. Math. 10 (2), 157–165.

Geng, J., Longhi, E., Behringer, R.P., Howell, D.W., 2001. Memory in two-dimensional heap experiments. Phys. Rev. E 64 (6), 060301.

Goldenberg, C., Goldhirsch, I., 2005. Friction enhances elasticity in granular solids. Nature 435 (7039), 188–191.

Goldenberg, C., Goldhirsch, I., 2008. Effects of friction and disorder on the quasistatic response of granular solids to a localized force. Phys. Rev. E 77 (4), 41303.

Goodey, R., Brown, C., Rotter, J., 2003. Verification of a 3-dimensional model for filling pressures in square thin-walled silos. Eng. Struct. 25 (14), 1773–1783.

Goodey, R., Brown, C., Rotter, J., 2006. Predicted patterns of filling pressures in thin-walled square silos. Eng. Struct. 28 (1), 109–119.

Holst, J.M.F.G., Ooi, J.Y., Rotter, J.M., Rong, G.H., 1999. Numerical modeling of silo filling. I: Continuum analyses. J. Eng. Mech. ASCE 125 (1), 94–103.

Huntley, J.M., 1999. Force distribution in an inhomogeneous sandpile. Eur. Phys. J. B 8 (3), 389–397.

Janbu, N., 1963. Soil compressibility as determined by oedometer and triaxial tests. In: Eur. Conf. Soil Mech. Found. Eng., Wiesbaden, Germany, 19–25.

Jeong, H.-Y., Moore, I.D., 2010. Calculations for central stress minimum under sand piles using continuum analysis. ZAMM 90 (1), 65–71.

Kulhawy, F., Duncan, J., 1972. Stresses and movements in Oroville dam. J. Soil Mech. Found Div. 98 (7), 653–665.

Liffman, K., Chan, D.Y.C., Hughes, B.D., 1994. On the stress depression under a sandpile. Powder Technol. 78 (3), 263.

Luding, S., 1997. Stress distribution in static two-dimensional granular model media in the absence of friction. Phys. Rev. E55 (4), 4720–4729.

Luding, S., 2005. Granular media Information propagation. Nature 435, 159–160.

Matuttis, H.G., 1998. Simulation of the pressure distribution under a two-dimensional heap of polygonal particles. Granul. Matter, 1 (2), 83–91.

McBride, W., 2006. Base pressure measurements under a scale model stockpile. Particul. Sci. Technol. 24 (1), 59–70.

Menetrey, P., William, K., 1995. Triaxial failure criterion for concrete and its generalization. ACI Struct. J. 92 (3).

Michalowski, R.L., Park, N., 2004. Admissible stress fields and arching in piles of sand. Geotechnique 54 (8), 529–538.

Modaressi, A., Boufellouh, S., Evesque, P., 1999. Modeling of stress distribution in granular piles: comparison with centrifuge experiments. CHAOS 9 (3), 523–543.

Ooi, J.Y., Rotter, J.M., 1990. Wall pressures in squat steel silos from simple finite element analysis. Comput. Struct. 37 (4), 361–374.

Ooi, J.Y., She, K.M., 1997. Finite element analysis of wall pressure in imperfect silos. Int. J. Solids Struct. 34 (16), 2061–2072.

Ooi, J., Chen, J., Lohnes, R., Rotter, J., 1996. Prediction of static wall pressures in coal silos. Constr. Build Mater. 10 (2), 109–116.

Ooi, J.Y., Al, J., Zhong, Z., Chen, J.F., Rotter, J.M., 2008. Progressive pressure measurements beneath a granular pile with and without base deflection. In: Chen, J.F., Ooi, J.Y., Teng, J.G. (Eds.), Structures and granular solids: from scientific principles to engineering applications. CRC Press, London, pp. 87–92.

Rotter, J.M., Holst, J.M.F.G., Ooi, J.Y., Sanad, A.M., 1998. Silo pressure predictions using discrete-element and finite-element analyses. Philos. Trans. Roy. Soc. A 356 (1747), 2685–2712.

Rowe, R.K., Skinner, G.D., 2001. Numerical analysis of geosynthetic reinforced retaining wall constructed on a layered soil foundation. Geotext. Geomembr. 19 (7), 387–412.

Savage, S.B., 1998. Modeling and granular material boundary value problems. Kluwer Academic Publishers, Physics of Dry Granular Media, 25–96.

Savage, S.B., 1997. Problems in the statics and dynamics of granular materials. In: Powders and Grains 97. Balkema, Rotterdam, Netherlands, pp. 185–194.

SIMULIA 2007. Abaqus Analysis: User's Manual. Dassault Systèmes.

Smid, J., Novosad, J., 1981. Pressure distribution under heaped bulk solids. Proceedings of 1981 Powtech. Conf., Ind. Chem. Eng. Symp., 63.

Tejchman, J., Wu, W., 2008. FE-calculations of stress distribution under prismatic and conical sandpiles within hypoplasticity. Granul. Matter 10 (5), 399–405.

Vanel, L., Howell, D., Clark, D., Behringer, R.P., Clément, E., 1999. Memories in sand: experimental tests of construction history on stress distributions under sandpiles. Phys. Rev. E 60 (5), R5040–5043.

Wittmer, J.P., Claudin, P., Cates, M.E., Bouchaud, J.P., 1996. An explanation for the central stress minimum in sand piles. Nature 382 (6589), 336–338.

Wu, W., Bauer, E., Kolymbas, D., 1996. Hypoplastic constitutive model with critical state for granular materials. Mech. Mater. 23 (1), 45–69.

Yu, S.K., 2004. Finite element prediction of wall pressures in silos (Ph.D. thesis). Built Environment Research Unit, The University of Wolverhampton, Wolverhampton, U.K.

Zimmermann, T., Truty, A., Urbanski, A., Commend, S., Podles, K., 2009. ZSOIL.PC: A unified approach to stability, bearing capacity, consolidation, creep and flow for two and three-dimensional simulations in geotechnical practice. White paper.

Zuriguel, I., Mullin, T., 2008. The role of particle shape on the stress distribution in a sandpile. Proc. Roy. Soc. A 464 (2089), 99–116.